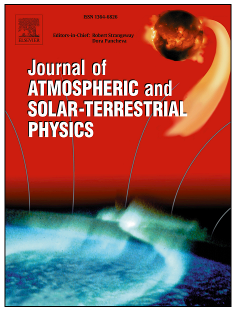

Temporal variations of PM concentrations, and its association with AOD and meteorology observed in Nanjing during the autumn and winter seasons of 2014–2017

Na Kang, Farong Deng, Rehana Khan, K. Raghavendra Kumar, Kang Hu, Xingna Yu, Xuelian Wang, N.S.M.P. Latha Devi

PII: S1364-6826(20)30090-0

DOI: https://doi.org/10.1016/j.jastp.2020.105273

Reference: ATP 105273

To appear in: *Journal of Atmospheric and Solar-Terrestrial Physics*

Received Date: 10 October 2019

Revised Date: 11 March 2020

Accepted Date: 26 March 2020

Graphical Abstract

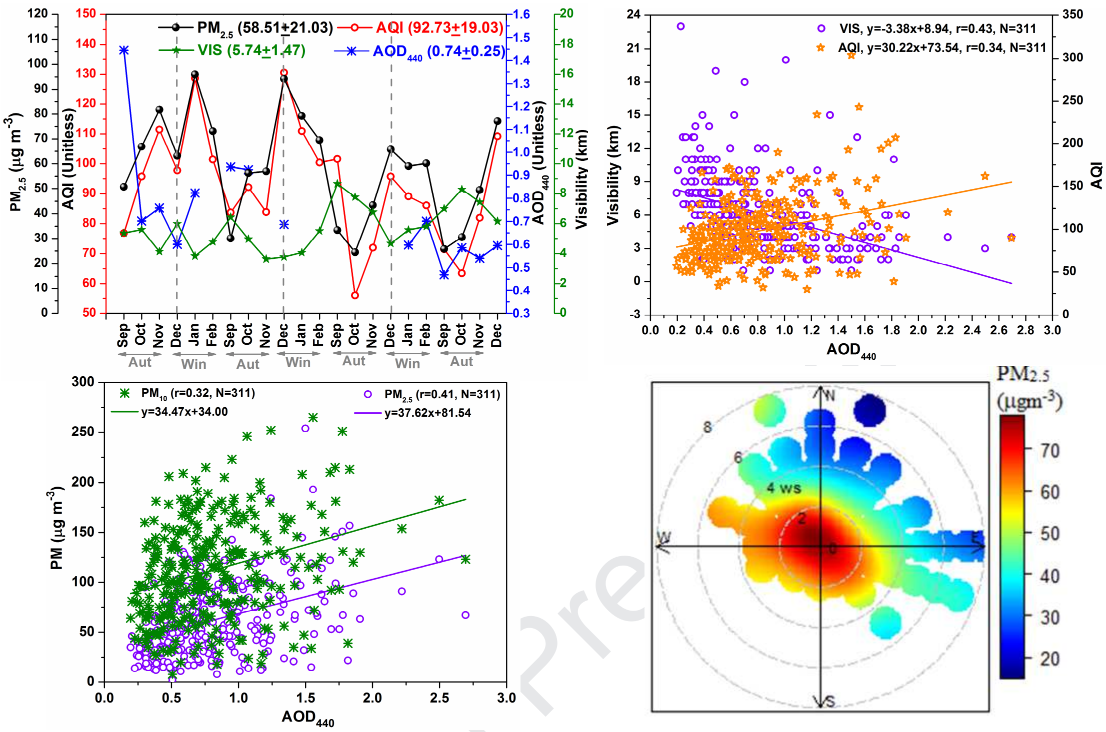

Temporal variations of PM concentrations, and its association with AOD and meteorology observed in Nanjing during the autumn and winter seasons of 2014-2017

Na Kang[a], Farong Deng[a], Rehana Khan[a,e], K. Raghavendra Kumar[b,a*],

Kang Hu[c], Xingna Yu[a], Xuelian Wang[d], N.S.M.P. Latha Devi[b]

[a]*Collaborative Innovation Centre on Forecast and Evaluation of Meteorological Disasters, Key Laboratory of Meteorological Disaster, Ministry of Education (KLME), International Joint Laboratory on Climate and Environment Change (ILCEC), Key Laboratory for Aerosol-Cloud-Precipitation of China Meteorological Administration, School of Atmospheric Physics, Nanjing University of Information Science and Technology, Nanjing 210044, Jiangsu, China.*

[b]*Department of Physics, School of Sciences and Humanities, Green Fields, Koneru Lakshmaiah Education Foundation (KLEF), K. L. University, Vaddeswaram 522502, Guntur, Andhra Pradesh, India.*

[c]*Department of Atmospheric Sciences, School of Earth Sciences, Zhejiang University, Hangzhou 310027, Zhejiang, China.*

[d]*Tianjin Institute of Meteorological Sciences, Tianjin, China.*

[e]*Department of Physics, Higher Education, Government of Khyber Pakhtunkhwa, Peshawar 25000, Pakistan.*

***Corresponding author**

Email: kanike.kumar@gmail.com; rkkanike@kluniversity.in (K. R. Kumar)

ABSTRACT

The present study aims to investigate temporal evolutions of particulate matter (PM) concentrations and its association with the meteorology and aerosol optical depth (AOD) during autumn and winter of 2014-2017 at an urban city, Nanjing in the Yangtze River Delta, East China. The seasonal mean $PM_{2.5}$ (PM_{10}) was found maximum and minimum with 81.2±41.5 µg m^{-3} (135.6±57.1 µg m^{-3}) and 33.7±19.1 µg m^{-3} (65.8±34.5 µg m^{-3}) during winter and autumn seasons, respectively. Furthermore, the mean ratio of $PM_{2.5}/PM_{10}$ was around ~0.57 for the entire study period, with a lower contribution (0.53) in autumn and higher (0.60) in winter. However, the seasonal mean AOD_{440}, precipitable water vapor content, Ångström exponent ($AE_{440-870}$) was found maximum with 0.97 ± 0.31, 1.58 ± 0.80 cm, and 1.14 ± 0.23 during autumn, and a minimum of 0.62 ± 0.34, 0.60 ± 0.27 cm, and 1.29 ± 0.19 in winter, respectively. The potential source contribution function (PSCF) and concentration weighted trajectory (CWT) models revealed considerable long-distance transport of $PM_{2.5}$ from north and northwest China. Besides, the concentration bivariate probability function (CBPF) revealed a significant contribution of $PM_{2.5}$ occurred when the winds blown from southerly and northwesterly directions. The relationship between $PM_{2.5}$ and meteorology found that $PM_{2.5}$ concentration had a positive relationship with AQI, while negative correlations with the major meteorological parameters. A notable spatial heterogeneities and trends were observed in AOD and AE, with negative correlations (-0.5 to 0) in winter over East China.

Keywords: Particulate matter; Meteorology; Aerosol optical depth; PSCF and CWT models.

1. Introduction

The importance of atmospheric aerosols such as particulate matter (PM) and cloud condensation nuclei (CCN) for the climate is well known and is an inevitable topic in Atmospheric Physics and Chemistry (Kalluri et al., 2016). They consist of solid or liquid particles suspended in the atmosphere with various sizes (1 nm-1 µm), and play a crucial role in weather and climate change. Aerosols (natural and anthropogenic) are often mixed, and can also be described by their size, e.g., PM_{10} are particles with aerodynamic diameters less than 10 µm, while $PM_{2.5}$ particles with aerodynamic diameters less than 2.5 µm. They affect the climate directly by scattering and absorbing solar radiation; and thereby, altering radiation budget at the top, surface and within the atmosphere, which in turn influences the atmospheric heating rate (Charlson et al., 1992). However, the long-term climatic effects lead to changes in aerosols optical properties, and microphysical properties of clouds including their lifetime, formation and precipitation (Twomey, 1997); and thereby, indirectly change terrestrial radiation. Further, many studies have shown that human health can be affected by long-term exposure to fine PM concentrations, particularly from $PM_{2.5}$ is associated with various diseases such as respiratory tract infections, asthma, and lung diseases, that eventually leads to visibility degradation with their increased concentration in the atmosphere (Pope et al., 2006).

With rapid economic development, urbanization, and industrialization, China has become one of the most polluted regions in Asia during recent decades. Since 2013, the China National Environmental Monitoring Center (CNEMC) has established numerous ground-based observation stations to measure several air pollutant concentrations, which are of great significance for the assessment of air quality in China (Hou et al., 2019). By the end of 2013, a national air quality monitoring network with more than 1500 stations in China is put into the operation, which provides air quality for the pollutants such as $PM_{2.5}$, PM_{10}, SO_2, NO_2, CO, O_3 to the public. The earth's environment is constantly evolving, owing to the increasing human population, and their corresponding activities leading to source emission of air pollutants. For example industrial activities, land use and combustion of fossil fuels emit greenhouse gases and aerosols, resulting in the change of atmospheric composition (Crowley et al., 2000) greatly due to their day by day variations. Subsequently, these factors badly affect air quality, human health, climate and environment (Tiwari et al., 2013; Zhang and Cao, 2015; Hou et al., 2019).

People from their fields studied the $PM_{2.5}$ and PM_{10} issues from various perspectives. A lot of publications were involved in the spatial distribution and seasonal/diurnal changes of PM and their association with aerosol optical depth (AOD) and key meteorological variables. For example, Han et al. (2014) have shown that urbanization played a considerable part in $PM_{2.5}$ concentrations that eventually leads to a significant influence on public health and air quality. Though much progress has been made, large discrepancies and knowledge gaps still exist among $PM_{2.5}$ and PM_{10}. However, several previous authors were noticed maximum concentrations in their recent studies during the autumn and winter seasons in China. Zhang and Cao (2015) noticed increased levels of $PM_{2.5}$ concentration during autumn and winter seasons over East China due to enhanced contribution from open biomass burning. Li et al. (2017) found higher values of $PM_{2.5}$ in autumn (85.5 μg m^{-3}) and winter (97.2 μg m^{-3}) compared to other seasons in an urban region of Northeast China. Similar results were reported by Shao et al. (2017) in Nanjing for the $PM_{2.5}$ observations during 2013-2015. Further, the recent investigation by Wang et al. (2017) on $PM_{2.5}$ and PM_{10} noticed high concentration in winter with the samples collected at an urban site of Zhengzhou, could be associated with an increase in air pollutants (due to the continuous usage of heating systems) and stable meteorological conditions. A recent study by

Hou et al. (2019) revealed that surface $PM_{2.5}$ concentrations were decreased during 2013-2018 over highly polluted areas due to a reduction in anthropogenic emissions, with stable values found over the Pearl River Delta region.

Even though, the previous investigations were dedicated to a specific location based on the large span of data covering all seasons and failed to present changes in PM concentrations to understand the mechanisms involved in haze-fog phenomena during autumn and winter seasons. Using the measured datasets provided by CNEMC, the present study aims to examine the temporal variability of $PM_{2.5}$ and PM_{10} concentrations and source transport analysis from multivariate statistical trajectory models such as potential source contribution function (PSCF) and concentration weighted trajectory (CWT) in conjunction with the concentration bivariate probability function (CBPF) analysis during autumn and winter of 2014-2017. This will allow the authors to examine the role played by the atmospheric circulations in understanding the haze-fog phenomena at an urban-industrial polluted city, Nanjing in the Yangtze River Delta (YRD) region, East China. Further, the paper focused to reveal the relationship and causes of changes in pollution between the aerosol optical properties and meteorological variables with the PM concentrations over the region. At last, we derived and presented the clustering results obtained from the identification and classification schemes to define different aerosol types, with a perspective to give some brief analysis on spatial changes and trends in AOD using the satellite data observed from the MODIS sensor.

2. Data and meteorology

2.1. Experimental station

The study area (Nanjing, 32.05° N, 118.78° E, 62 m above sea level) lies on the left bank of the Yangtze River Delta (YRD) region and is located in the Jiangsu province, East China. The city lies at an altitude of 83 m above sea level and is surrounded by several iron, steel and power generation plants located within the proximity of ~5-7 km in the northeast of the measurement site. Besides, the region suffers from both the heavy traffic and the agglomeration of heavy industry. The climatological annual mean temperature and total precipitation in the region were about 15-17º C and 1000-1200 mm, respectively, with a maximum occurrence during the summer. However, the prevailing winds are southeasterly in summer and northeasterly in winter derived from the Siberian anticyclone (Chen et al., 2018). More details about the layout of the site, meteorology, and aerosol types and sources can be found elsewhere (Yu et al., 2016; Kang et al., 2016a, b) and will be discussed in the following sections for the present database.

2.2. Air pollutant data

Real-time hourly monitoring data of $PM_{2.5}$ and PM_{10} mass concentrations in China between September 2014 and February 2017 are available from the China air quality online monitoring and analysis platform (https://www.aqistudy.cn/) and the Ministry of Environmental Protection of China (http://106.37.208.233:20035/). All the measurement sites in Nanjing were equipped with the Tapered Element Oscillating Microbalance (TEOM, RP1400 Model) instruments from Thermo Scientific Company, USA to measure the main atmospheric air pollutant concentrations at a resolution of 0.1 μg m^{-3} (Hou et al., 2019).

As a vertical integral, AOD not only reflects the impact of aerosols on the environment and climate on the surface but also reflects the impact of aerosols at different heights of the boundary layer as well, even in the upper and middle troposphere. In this study, the level 2 Collection 6.0 daily averaged AOD at 550 nm derived from the MODIS sensor onboard the Aqua satellite is obtained from the NASA GIOVANNI (https://giovanni.gsfc.nasa.gov/giovanni/) for the period during September 2014–February 2017. The downloaded MODIS AOD data are averaged into the seasonal and annual AOD values and are used to supplement the measured pollutant data.

2.3. Meteorological parameters

Nanjing has a humid subtropical climate with hot summers and cold winters. Moderate to low rates of air temperatures and precipitation were recorded during the autumn (from September to November) and winter seasons (from December to January) throughout the study period. The meteorological parameters include, air temperature (AT in ºC), relative humidity (RH in %), rainfall (RF in mm), wind speed (WS in m s^{-1}), and wind direction (WD in deg) to some extent exert a strong influence on PM concentrations. The 24-h daily average meteorological parameters for the period 2014-2017 were procured from http://wunderground.com, a world-wide-web based meteorological variables for a geographical area, and previously been used by other researchers (e.g., Kang et al., 2016a, b).

Fig. S1 of Supplementary Material (SM) shows the changes in air temperature, relative humidity, and rainfall observed at Nanjing during autumn and winter for the period 2014-2017. The monthly mean ambient air temperature found maximum in September 2016 (23 °C) and minimum in January 2018 (AT< 3 °C) due to the frequent occurrence of haze and fog conditions (Kang et al., 2016b) over the region. Whereas, the RH (relative humidity) was recorded highest in October 2016 (>85%) and lowest in December 2014 (<59%) causing dry conditions attributed to low water vapor and weak winds. It is obvious that both the parameters had depicted the opposite trend in winter, with a similar variation in autumn. However, previous studies (Gao et al., 2008, Yang et al., 2013) suggested that changes in meteorological conditions, regional urbanization, and land use can cause the temperature to rise and RH to decrease, which result mostly in more haze-fog conditions and less precipitation in China. It is also inferred from Fig.

S1 of SM that the precipitation rate reaches a maximum in the autumn of 2016 (> 195 mm), with an increase of temperature. Moreover, it is revealed that the precipitation was found directly related to the air temperature, with an increase of temperature results in an increase in the rate of precipitation also, at the study site.

Fig. S1 of SM also presents the wind rose plots to analyze the relative frequency of wind speed in autumn, winter, and autumn+winter at Nanjing for the period 2014-2017. The wind rose shows the direction of wind blowing, while the color gives the magnitude of binned wind speed. It is found that the direction of winds in autumn and winter seasons was dominated by the winds coming from south and southeast directions. The strong (6 ms^{-1}) southeasterly winds bring air masses, which may possess a large fraction of anthropogenic aerosols, significantly influence the regional climate. Since the wind experienced at any given location is highly dependent on local topography and meteorological factors.

3. Data processing methods

3.1. Spectral dependence of AOD and AE

A very brief description about the aerosol optical and physical parameters is given here since several previous studies (e.g., Eck et al., 1999; Kaskaoutis et al., 2009; Kumar et al., 2013) have described the physical significance, its use and derivation, which confirm to the applied statistics and instrument algorithm. The spectrally-dependent AE parameter provides useful information about the particle-size computed from the AOD using any pair of wavelengths given by the Ångström law (Ångström, 1961);

$$AOD_{\lambda} = \beta\lambda^{-AE} \quad (1)$$

where 'λ' (in µm) is the wavelength. The Ångström turbidity cœfficient (β) varied in the range 0–1, and acts as an indicator of the number of aerosols present in the atmospheric column, being equal to AOD (λ) at λ=1 µm.

Also, the Volz's method can be applied to any pair of wavelengths in the spectral AOD for the computation of AE. It relies on the Junge power law and its value is a qualitative indicator of aerosol particle-size (Kumar et al., 2013) where AE < 1.0 and > 1.0 represents the dominance of coarse- and fine-mode, respectively in the aerosol size distribution. In the present study, AE was estimated in the range 440–870 nm from the following equation:

$$AE = -\frac{d \ln AOD_{\lambda}}{d \ln_{\lambda}} = \frac{\ln\left(\frac{AOD_{\lambda_1}}{AOD_{\lambda_1}}\right)}{\ln\left(\frac{\lambda_1}{\lambda_2}\right)} \qquad (2)$$

where AOD_{λ_1} and AOD_{λ_2} represent AOD at two wavelengths λ_1 and λ_2, respectively.

3.2. Multivariate statistical trajectory models

3.2.1. HYSPLIT Trajectory analysis

The analysis of the movement of air parcels can be easily quantified utilizing the trajectory model. This technique is much effective in identifying the transport carries source receptor from one place to the other following the forward and backward calculations. There are some limitations in the trajectories, which involves majorly grid resolution of input data. The reanalysis data, forecast data at various grid resolutions in both spatial and vertical, gives a deviation in the air mass trajectories. To defend this problem, there can be some other trajectory statistical analysis models such as PSCF and CWT (Wang et al., 2010) which are discussed in the upcoming sections. In the present study, air mass backward trajectories arriving at Nanjing originated at a height of 500 m above ground level ending at 12:00 h UTC with 120 h duration of time. These trajectories were calculated every 6 h (00:00, 06:00, 12:00, and 18:00 h UTC) using the NOAA's version 4 of Hybrid Single-Particle Lagrangian Integrated Trajectory (HYSPLIT-4) model (Draxler and Rolph, 1997), which is a widely used model for analyzing and calculating the transport of air pollutants.

3.2.2. The PSCF model

The potential source areas can be identified by using the PSCF method, which combines the backward trajectory and defined values of air pollutants (Wang et al., 2009). The study field is divided into small equal grid cells (ij). The value of PSCF is expressed as:

$$PSCF_{ij} = \frac{m_{ij}}{n_{ij}} \quad (3)$$

where i and j denote the latitude and longitude, respectively, n_{ij} represents the total number of endpoints passing through the ij cell, and m_{ij} is defined as the number of endpoints in the same cell associated with samples that are higher than the criterion value. The 75th percentile for each chemical species is selected as the criterion value for m_{ij}. The PSCF value represents a conditional probability describing the potential contribution of a grid cell of the high pollutant loadings at the receptor site. Cells with high PSCF values indicate areas of high potential contributions to the pollutant concentration at the receptor site, and the trajectories passing through these cells are the major transport pathways leading to the high pollutant loadings at the receptor site. To reduce the uncertainty in cells, a weighting function w (n_{ij}) should be multiplied with the PSCF value when n_{ij} is lower than three times an average number of trajectory endpoints (n_{mean}) in each cell (Zeng and Hopke, 1989). The weighted potential source contribution function (WPSCF) is described as follows:

$$WPSCF_{ij} = \frac{m_{ij}}{n_{ij}} \times W\left(n_{ij}\right) \quad (4)$$

The weight function W_{ij} is defined as:

$$w_{ij} = \begin{cases} 1.00 & n_{ij} > 3.Avg \\ 0.70 & Avg < n_{ij} \le 3.Avg \\ 0.42 & 0.5.Avg < n_{ij} \le Avg \\ 0.17 & n_{ij} \le 0.5.Avg \end{cases} \quad (5)$$

where Avg is the average number of endpoints in each cell.

3.2.3. The CWT model

The CWT method, developed by Hsu et al. (2003), was used to make a distinction between strong sources from weak ones, considering the limitation of the PSCF method in which grid cells can have the same PSCF value when the sample concentrations are either only slightly higher or much higher than the criterion. In the CWT method, each grid cell is assigned a weighted concentration by averaging the sample concentrations that have associated trajectories that crossed the grid cell as follows:

$$C_{ij} = \frac{\sum_{h=1}^{M} C_h \times \tau_{ijh}}{\sum_{h=1}^{M} \tau_{ijh}} \times W(n_{ij}) \quad (6)$$

where C_{ij} is the mean weight concentration of the back trajectory 'h' in the ij cell; C_h represents $PM_{2.5}$ concentration in the trajectory 'h' through ij cell; τ_{ijh} represents the actual time that trajectory 'h' resides in the ij cell. Besides, W (n_{ij}) used in CWT is the same as that in PSCF to reduce the uncertainty in cells.

Both WPSCF and WCWT analyses were calculated using the MeteoInfo software-TrajStat Plugin (Wang et al., 2009), which has been proven useful to identify potential source areas of $PM_{2.5}$ and its chemical species.

3.3. *Discrimination of aerosol types*

An investigation of major aerosol types were identified over urban Nanjing site via., the AOD_{440} versus $AE_{440\text{-}870}$ cluster technique previously used in several studies (Kaskaoutis et al., 2009; Bibi et al., 2016; Patel et al., 2017; Boiyo et al., 2018; Kumar et al., 2018). The method is based on the sensitivity of the two wavelength-dependent parameters (AOD and AE) to discriminate different aerosol types following the defined threshold value which varies depending on the geographical locations (Pace et al., 2006). In the present work, AOD_{440} and $AE_{440\text{-}870}$ values were in the range of 0.1–1.9 and 0.4–1.8, respectively. Therefore, the values of $AOD < 0.15$ and $AE < 0.9$ are represented as the clean maritime (MA) aerosol type. On the other hand, $AOD < 0.15$ and $AE > 1.0$ is used for the polluted continental (PC) type of aerosols. However, $AOD > 0.3$ and $AE > 1.0$ are characterized as the urban-industrial/biomass burning (UI/BB), while, $AOD > 0.6$ with $AE < 0.7$ indicated the desert dust (DD) aerosol types. The remaining gaps were considered as a mixed type of aerosols (MX). The MX aerosols are difficult to be discriminated against, bearing in mind the distinct effects of various aerosol-mixing processes in the atmosphere such as coagulation, condensation, humidification, and gas-to-particle conversion (Kaskaoutis et al., 2009).

3.4. *Aerosol modification scheme*

The AE is dependent on the spectral band used for its estimation and reflects different aerosol-types (Eck et al., 1999). At shorter wavelengths, it provides information regarding size variation of fine-mode particles; while at longer wavelengths, it yields information about the variation in fine- to the coarse-mode ratio (Kumar et al., 2013). The aerosol modification processes at Nanjing were examined using the graphical scheme proposed by Gobbi et al. (2007) and utilized by several authors (Kaskaoutis et al., 2011; Yu et al., 2016; Kang et al., 2016b; Patel et al., 2017; Boiyo et al., 2018). The method relies on the combined analysis of $AE_{440-870}$ and its spectral curvature represented by $dAE = AE_{440-675} - AE_{675-870}$ with fine-mode effective radii (R_f) and FMF (η) as grid parameters in a grouped AOD. The graphical framework has been drawn using Mie theory for a typical refractive index of air m=1.4–0.001i. More details concerning the scheme and sensitivity analysis are discussed by Gobbi et al. (2007).

The change in AE (dAE) pairs with increasing $AOD_{675\ nm}$ provides crucial information regarding aerosol-modification processes in the atmosphere (i.e., cloud contamination, hydration, and coagulation) (Kumar et al., 2014). Negative values of dAE are associated with negative curvature (i.e., larger values of AE indicate the dominance of fine-mode particles). Positive values are associated with positive curvature (i.e., smaller values of AE suggest the dominance of coarse-mode particles associated with bimodal size distribution). A zero value of dAE represents the absence of AE spectral variability (Kaskaoutis et al., 2011). Therefore, to investigate the spectral variation of AE, its difference (dAE) at shorter (440–675 nm) and longer (675–870 nm) wavelength are calculated and plotted against $AE_{440–870}$ as a function of AOD_{675}. The aerosol modification processes in Nanjing were examined using daily averaged observations of AE and AODs, with the latter (at 675 nm) represented by different colors and symbol size of increasing turbidity.

3. Results and discussion

3.1. Frequency distributions

The frequency distributions of $PM_{2.5}$, PMr, AOD_{440}, and $AE_{440-870}$ during the two seasons for the entire study period are shown in Fig. 1. The bin interval in the present study was set to 0.1 for PMr, AOD_{440}, and $AE_{440-870}$, and 10 for $PM_{2.5}$. However, we considered daily averaged values of $PM_{2.5}$ and AOD_{440} in the range 0–260 µg m^{-3}, and 0–3.3 respectively, while 0–1.8 for

PMr, and $AE_{440-870}$, respectively. The $PM_{2.5}$ showed a wide unimodal distribution, with significant seasonal heterogeneity (Fig. 1a) attributed to complex seasonal patterns (as for thermal inversion and foggy conditions) of the atmosphere and variability in meteorological phenomena (Che et al., 2014). The $PM_{2.5}$ autumn season peaked at a bin interval of 20–40 μg m^{-3}, accounting for 33.50% of the total distribution. On the other hand, it showed the strongest mode in the bin interval of 40-60 μg m^{-3} contributing 21.5%, signifying the dominance of absorbing fine aerosol type during winter. Furthermore, PMr distribution significantly skewed towards larger values (Fig. 1b) in both seasons throughout the study period is more likely related to large seasonal heterogeneity and massive biomass burning in the YRD. In autumn, almost 60% of the values were in the interval of 0.4-0.6; whereas, in winter, nearly 48% of the values were found between 0.6 and 0.8, indicating that PM_{10} concentrations were found considerably higher than $PM_{2.5}$. In both the seasons, AOD_{440} showed the strongest modes in the bin interval of 0.4–0.6 (autumn) and 0.6-0.8 (winter), accounting for 25.1% and 25.5%, respectively (Fig. 1c). Meanwhile, the $AE_{440-870}$ also illustrated a sharp peak at larger values (>1.0), with its wide distribution (Fig. 1d) similar to the results reported by Kang et al. (2016a) and Kumar et al. (2018) over Nanjing using the MODIS satellite data. The occurrence of strong modes at relatively higher size bins, with seasonal means > 1.0 (Table 1) during both the seasons interprets more contribution of fine- relative to coarse-mode particles.

3.2. Temporal changes in PM and AOD

The seasonal mean AOD_{440} was found high with 0.97 ± 0.31 and 0.86 ± 0.45 during autumn and winter of 2015, respectively (Table 1). However, the annual mean values of AOD_{440} for the entire study period was 0.74 ± 0.25 (Fig. 2), which is higher compared to that recorded at other sites (Kaskaoutis et al., 2009; Kumar et al., 2013; Bibi et al., 2016; Patel et al., 2017; Boiyo et al., 2018). Further, the mean AOD_{500} value of 0.65 ± 0.14 observed during winter reported by Srivastava et al. (2014) at an urban Delhi is comparable with our findings obtained in this study. Moreover, the MODIS AOD_{550} was found close to 0.9, while the Cimel Sunphotometer (CSP) measured AOD_{440} showed a high value of 1.48, with a mean of 0.74 ± 0.25 for the study area.

The monthly mean precipitable water vapor content (PWC) (Fig. 2a) varied from 0.48 to 3.40 cm, with its seasonal mean found highest (1.58±0.80 cm) in autumn during the study period observed at Nanjing. The PWC was recorded very high (3.4 cm) in September 2014 with the AOD and PWC almost followed a similar pattern, except in 2017 with each other, which signifies the hydrophilic nature of the aerosol particles on the humid regions of East China. This aspect implies that the higher amount of water content helped the growth of existing particles, and subsequently results in the formation of new particles in the same vicinity, which in turn results in higher AOD (Kumar et al., 2013).

The annual mean $AE_{440\text{-}870}$ was found 1.14 ± 0.13 for the study area (Fig. 2b). However, AE was found low (< 1.0) during winter indicates the presence of mixed aerosols with the dominance of fine- particles. Even, it increased to 1.1 in the other years of study attributed to enhanced anthropogenic activities; and sometimes reached maximum values around 1.4 due to intense biomass burning in the vicinity of the study region. However, the contribution from the windblown mineral dust aerosols from the surrounding continents due to long-range transport cannot be ruled out. Whereas, the mean value of β was estimated to be about 0.31 ± 0.12 during the period 2014-2017 (Fig. 2b). The aerosol loading was extremely high (0.65) at the initial period of study in September 2014 but suddenly dropped down to 0.15 during September 2017 resulting in decreased aerosol concentrations attributed to strict implementation of new environmental policies in China (Hu et al., 2018), apart from the meteorological phenomena.

The monthly mean $PM_{2.5}$ was found moderate (22 µg m^{-3}) to high (98 µg m^{-3}), with an annual mean of 58.51 ± 21.03 µg m^{-3} over the study region during 2014-2017. We found maximum values of annual $PM_{2.5}$ in winter (81.2±41.5 µg m^{-3}) compared to the autumn, with monthly mean larger values noticed in January 2015 and smaller in October 2016. The increased concentrations of $PM_{2.5}$ in winter are attributed to biomass and fossil fuel burning (Wang et al., 2014; Chen et al., 2019). Also, less amount of precipitation and lower wind speed during winter results in the maximum concentration of $PM_{2.5}$ over the study site. This results in the deterioration of air quality over the region (Tao et al., 2014). Also, a high density of fire spots was noticed closer to Nanjing resulting in high $PM_{2.5}$ and more amounts of absorption aerosols. Apart from these, the urban, industrial and vehicle emissions play an important role for higher PM concentrations in some cities (Cheng et al., 2012). The AQI follows a similar pattern as that of $PM_{2.5}$ throughout the study; whereas, the visibility noticed opposite variation with $PM_{2.5}$ indicating an increase in $PM_{2.5}$ resulted in a decrease of visibility, and vice-versa. Furthermore, the seasonal ratio in $PM_{2.5}/PM_{10}$ was found to be lower (0.53) in autumn and higher (0.60) in winter seasons, with an annual mean of 0.57 (Table 1) attributed to the dominance of fine particles. Sharma and Maloo (2005) reported similar values (~0.58) at three different sampling locations in Kanpur, a highly polluted city in the northern part of India during the winter of 2002-2003. Tiwari et al. (2009) also reported the PM ratio (0.48±0.21) varying between 0.18 (June) and 0.86 (February) across Delhi, suggested the dominance of fine-mode particles in winter.

3.3. Source analysis from trajectory models

The PSCF and CWT models were used to reveal the potential origins of $PM_{2.5}$ geographically. To investigate the aerosol sources from its pathways during different seasons arriving in Nanjing, the weighted analyses of PSCF and CWT models for $PM_{2.5}$ are performed on a seasonal and annual basis (Fig. 3). Since, weighted-PSCF (WPSCF) is a method for estimating the potential source locations for long-range transported pollutants, such as $PM_{2.5}$ (Tao et al., 2014). However, the PSCF cluster analysis suggested that potential sources of $PM_{2.5}$ over the study region are local as well as transported from distant places, mostly situated in north and northwest of the observation site. This depends on the meteorological conditions and regional anthropogenic activities that vary 0.1-0.5 with the season. The reason is most of the cities located along the YRD are industrial as well as regional transport from these areas would have a potentially high impact on the formation of $PM_{2.5}$ (Zong et al., 2018). Furthermore, the weighted-CWT (WCWT) was also performed, to determine the possible emission sources causing $PM_{2.5}$ variability at the receptor site. The seasonal mean WCWT values of > 40 µg m^{-3} and > 80 µg m^{-3} revealed large influence of potential regional sources of aerosols originating from the north and northwest of measurement site during autumn and winter, respectively; while the small source of aerosols transporting from the East influenced with the WCWT of < 20 µg m^{-3} was found on an annual scale. This emphasizes the contribution of coarse particles, typically originated from the upper parts of Jiangsu region located in East China. However, the air masses in autumn and winter seasons were mostly originated from the northwestern directions, carrying similar types of aerosols.

3.4. Relationship between surface and column aerosols

The scatter plots of PM pollutant concentrations versus PM_{10}, PMr, and AOD_{440} observed at Nanjing during 2014-2017 are considered for correlation studies (Fig. 4). With the corresponding linear regressions (using daily averages), significant strong correlations were observed between $PM_{2.5}$ (0.94), $PM_{10-2.5}$ (0.82) and PM_{10} (Fig. 4a) indicates the dominant sources of fine and inhalable particles in Nanjing have similar origins (such as direct motor vehicle emissions and suspended road dust). It is revealed from the slope observed between $PM_{2.5}$ and PM_{10} (0.67) indicates the PM ratio is dominant with fine-mode particles in Nanjing. The regression analysis between mass concentrations of PM versus daily values of PMr is plotted in Fig. 4b. Among the three PM pollutants, $PM_{2.5}$ exhibited a fair correlation of 0.54 with PMr indicating a significant contribution of $PM_{2.5}$ in the PM ratio. It is observed that the $PM_{2.5}$ and PM_{10} are positively correlated with PMr, except $PM_{10-2.5}$ which showed a negative relationship. The correlation was found relatively low for PM_{10} (0.26) with PMr due to the high variability, although it was slightly better (0.32) with AOD_{440} (Fig. 4c). However, both $PM_{2.5}$ (0.41) and PM_{10} (0.32) showed positive correlations with AOD observed during the study period, with later relatively weak than the former pollutant.

3.6. Association between AOD, $PM_{2.5}$, and meteorology

Fig. 5 illustrates the scatter plots to present the relationships between column AOD and meteorological parameters. The intercept in the regression equation represents the background air temperature and slope represents a coefficient used for converting AOD in temperature (°C) and relative humidity (%). However, Fig. 5a provides the correlation between RH and temperature with intercept values of 63.80 and 10.61, respectively and correlation coefficients of 0.24 and 0.06, respectively during the study period over Nanjing. This is likely a result of the common trends of human activities during this time. Another reason is that the site receives usually heavy rainfall during the summer and autumn seasons that subsequently causes the temperature to fall and increases RH.

Regression analysis between the precipitation and wind speed versus AOD_{440} is shown in Fig. 5b. The resultant linear fitting has a slope of -3.62 and 0.09, and an intercept of 10.01 and

2.12 for precipitation and wind speed, respectively against AOD_{440}. Moreover, the correlation between AOD_{440} and precipitation was found weak (0.04). Also, a low intercept of 8.94 km was observed between visibility versus AOD_{440} (Fig. 5c), with a correlation coefficient of 0.43. However, all the meteorological parameters were found negatively correlated with $PM_{2.5}$ (Table 2), presenting the strong and weak correlations with visibility (-0.58) and rainfall (-0.09). In an early study by Fu et al. (2014) reported that wind speed is an important factor influencing $PM_{2.5}$. However, the wind speed can affect the accumulation and diffusion of aerosol particles; and the quantity $PM_{2.5}$ impinge on the visibility. The direction of the wind can affect the transport of pollutants and can determine the spatial distribution of visibility (Tao et al., 2014). However, the temporal trends of low visibility are mainly affected by the emissions of pollutants, aerosol compositions and meteorological conditions (Che et al., 2014).

3.7. Influence of winds on $PM_{2.5}$ concentration

The bivariate polar plots are shown in Fig. 6 presented the season-wise mean concentration of $PM_{2.5}$. The wind speed and direction were used to identify the sources responsible for $PM_{2.5}$ concentrations. In both the seasons, the high $PM_{2.5}$ concentrations were associated with lower wind speeds indicating the presence of local pollutants. But for the combined seasonal analysis (Fig. 6c) during the entire period of study, the highest concentrations were found mostly due to strong winds representing the presence of local emissions as well as long-range transported aerosols. In winter, air masses with a maximum concentration of particles are transported from almost every quadrant i.e., with high wind speed from the northwest (6 ms^{-1}), and comparatively low from northeast (2 ms^{-1}), southwest (4 ms^{-1}) and southeast (3 ms^{-1}) directions. Furthermore, the air masses showed bi-directional pathways from the southwest and northeast in autumn. However, $PM_{2.5}$ had higher concentrations in all directions during the autumn and winter seasons with low wind speed (< 4 m/s), which does not favor the dilution and dispersion processes of pollutants. Most importantly, higher concentrations of $PM_{2.5}$ in winter are associated with vehicular emissions. Eventually, the study area is also influenced by the highest $PM_{2.5}$ concentrations with the moderate breeze in autumn and winter seasons. This indicates the influence of emissions from an industrial area as well (a few km distances away from the study region) affecting the $PM_{2.5}$ concentrations. Similar results were also found for $PM_{2.5}$ over Thiruvananthapuram (India) (Sumesh et al., 2018) during winter and autumn seasons, suggesting that such a trend tends to be a general feature over India during the winter period with a large contribution of industrial aerosols.

3.9. Aerosol classification and modification processes

3.9.1. Identification of aerosol types

Fig. 7 shows the scatter plot of AOD versus AE to represent the major aerosol types with their seasonal percentage contributions at Nanjing. There is a wide range of AE values for low-to-moderate values of AOD reflecting large variability in the aerosol properties and suggesting several types of aerosols mixed in the atmosphere over Nanjing. The UI/BB type of aerosols was found the most contributors (>75%) reaching a maximum in winter (76.8%), indicating high turbid conditions due to enhanced fine-mode particles produced from the burning of fossil fuel and biomass (agricultural residue) or urban-industrial aerosols at the study area. A recent study by Kumar et al (2018) has found about 60.9% of anthropogenic contribution with the dominance of UI/BB aerosol type based on 12 years of MODIS AOD obtained over Nanjing. However, due to the neighboring arid regions in South China and Asia (that emit large amounts of dust in spring), the DD aerosols possess an important factor of 2.8% during autumn+winter (combined) and comparatively less in winter (~0.9%). Furthermore, MA and PC aerosol types hold no significant fraction over the study region; and no visible contribution has been found throughout the study period at Nanjing. However, cases that do not belong to any of the above categories are characterized as mixed (MX) types of aerosols were found to be 38.1%, 22.3%, 24.7% for the autumn, winter, and autumn+winter, respectively.

3.9.2. Aerosol classification scheme

Over the entire study region, nearly all the points are within the classification scheme represented as a function of AOD_{675} with different colors is shown in Fig. 7. The fine-mode particles are dominated in autumn, while some coarse-mode particles are observed in winter with a limited contribution during autumn+winter. This could be attributed to some dust particles associated with prolonged dry and cold winters in Nanjing. During autumn, decreasing AOD shows a shift to larger values of $AE_{440\text{-}870}$ (0.9–1.1) with R_f between 0.10 and 0.15 μm. Furthermore, a similar trend has been found in winter which is inconsistent with the recent findings of Patel et al. (2017) and Boiyo et al. (2018). However, with high AE (> 1.6), η ~90% and very low (< 0) values of dAE during winter interpret predominance of the same fine mode particles indicates hygroscopic growth of fine mode aerosols or increase in fine mode particles significantly due to cold breezes in winter (Kang et al., 2016b). The negative dAE indicates that these aerosols are of the bimodal distribution having a large fine-mode fraction (between 0.2 and 0.15). While negative dAE values with η > 70 %, suggesting a predominance of fine-mode particles, likely due to biomass burning activities and urban-industrial aerosols (Boiyo et al., 2018). In contrast to the separate analysis of autumn and winter seasons, the combined (autumn+winter) data set gives slightly different results with high AE (>1.5), η < 90% and 0.2-0.15 values of R_f, which interprets again the predominance of fine mode particles. However, a slightly lower inhomogeneity with significant contributions of various aerosol types (AOD ~

1.2–1.8) was found in winter and autumn plots. Similar results were also found over the Bay of Bengal (Kaskaoutis et al., 2011) and urban Hyderabad (Sinha et al., 2012) for the same seasons. It can, therefore, be interpreted that high AODs at Nanjing may be associated with increased concentration of particularly, fine mode particles, and were significantly contaminated by clouds. Moreover, the fine-mode particles are dominated in autumn and winter seasons particularly, the coarse-mode particles are observed with a limited contribution during the autumn and winter seasons.

3.8. Spatial variations and trends in AOD and AE

The optical parameter AOD is very useful for regional evaluation and investigating the characteristics of aerosols, atmospheric pollution and environment (Eck et al., 1999). The spatial distribution of AOD_{550} showed >0.70 (Fig. 8) in autumn for the study area, was higher than that in the surrounding area during the study period. However, higher values of AOD (≥0.7) were found in the East of the study region (between 32ºN to 34ºN and 121ºE to 122ºE). In the center towards the south part of Nanjing (between 26ºN to 31ºN and 116ºE to 118ºE), moderate aerosol concentrations (0.3< AOD < 0.6) were noticed, and clean environment conditions with AOD_{550} < 0.3 were found often in the southeast of the study area. Further, it is revealed that the seasonal averaged AOD in winter observed during 2014-2017 noticed higher than in autumn, and is more widely distributed in Jiangsu province. The spatial distributions of AE showed for winter and autumn seasons indicated a remarkably large amount of fine-mode aerosols in the north and west of the study region (Nanjing) attributed largely from biomass burning, and mixed aerosol in central and East of the study area, respectively.

The annual spatial trend distributions of AOD and AE (Fig. 9) are evaluated for two different seasons and combined during 2014-2017. We found positive trends in the east of the study region, with a negative trend in the north and other areas surrounding the study site. The significant positive trends in winter for the study period around the site are attributed to large anthropogenic activities and biomass burning. Even there are significant differences in the AE spatial variability between seasonal and annual means. The AE was found almost higher during the annual time than in the seasonal mean, especially during winter at the study site.

Fig. S3 of SM shows the spatial correlation analysis of AOD and AE values in eastern China from 2014 to 2017. The spatial correlation values in autumn were found to be similar to the spatial correlation between AOD and AE values in autumn+winter (combined) for the study period. Moreover, most of the regions were found with a positive correlation of ~0.6, ranging from 0 to 0.7. However, the spatial correlation was found negative in winter near the study region ranging from -0.5 to 0. Furthermore, our results are agreement with the findings of Mamun et al. (2014) investigated over the northern and southern parts (Chittagong division) of Bangladesh using the MODIS data from 2004 to 2013. They found the correlation coefficient of -0.94 between AOD and AE and RMSE as 0.09.

4. Conclusions

Monitoring and estimating the air pollutant concentrations are essential for evaluating air quality and its effects on the climate, environment, and human health. This study aims to examine the potential characteristics of the surface measured PM ($PM_{2.5}$ and PM_{10}) concentration and its association with column AOD and meteorological variables during autumn and winter seasons of 2014-2017 over Nanjing in the YRD region, East China. The annual mean values of $PM_{2.5}$ and PM_{10} in autumn (winter) were observed as 45.8±29.3 $\mu g\ m^{-3}$ (74.1±42.4 $\mu g\ m^{-3}$) and 83.5±45.1 $\mu g\ m^{-3}$ (120.9±56.6 $\mu g\ m^{-3}$), respectively during the study period. The observations showed with high values of $PM_{2.5}$ and PM_{10} exceeding the national air quality standards greatly and significantly affecting the visibility, air quality, and climate system. Further, the mean ratio of $PM_{2.5}/PM_{10}$ was about 0.57, with the lowest (0.53) observed in autumn and highest (0.60) during winter for the entire period. This revealed the dominance of fine-mode particles at Nanjing, attributed to anthropogenic activities (biomass burning, urban-industrial, vehicular emissions, and other pollutants generated by construction activities) and conducive meteorological phenomena. These resulting in serious pollution episodes at different locations in the YRD are likely related to several anthropogenic activities.

Different statistical techniques include the effect and temporal variation of winds through the CBPF analysis was used to analyze $PM_{2.5}$ in the study area. The bivariate plot results showed an increase in $PM_{2.5}$ concentration attributed to the presence of local anthropogenic emissions and favorable meteorological conditions over the study region. Apart from this, the source identification was carried out from the PSCF and CWT models utilizing the air mass trajectories obtained from the HYSPLIT model. The results showed that the regional transport of smoke particles from biomass-burning resulting in high surface PM concentration and column AOD. The present study also aims to investigate spatiotemporal evolution and trend in the aerosol optical properties, qualitatively identify different aerosol types and sources in Nanjing. For this purpose, the Collection 6 Level-2 data obtained from the MODIS sensor onboard Terra and Aqua satellites for the period between 2014 and 2017 have been analyzed. A notable spatiotemporal heterogeneity was observed in the optical properties of aerosols on the seasonal scale over Nanjing. The seasonal mean AOD_{440} ($AE_{470-870}$) was found to be maximum with 0.97 ± 0.31 during autumn (1.14 ± 0.23) and a minimum of 0.62 ± 0.34 (1.29±0.19) in winter. However, the spatial correlation between AOD and AE was found to be negative during winter, with the correlation coefficient ranging from -0.5 to 0. The results derived in this study contribute to an in-depth understanding of PM concentrations during autumn and winter seasons in urban Nanjing and forms a basis for the extension of future research over this aerosol hotspot region (YRD) in China.

Conflicts of interest

The authors declare and confirm that we don't have any competing financial interest concerning this study.

Funding Support

This work was financially supported by the National Natural Science Foundation of China (Grant Nos. 41805121, 41775123), the National Key Research and Development Program (Grant No. 2019YFC0214604), and the Natural Science Foundation of Tianjin City (Grant No. 16JCYBJC21500). The authors KRK and NSMPLD are grateful to the Department of Science and Technology (DST), Govt. of India for the award of DST-FIST Level-1 (SR/FST/PS-1/2018/35) scheme to Department of Physics, KLEF.

Acknowledgments

We acknowledge the Ministry of Environmental Protection of China (http://113.108.142.147:20,035/emcpublish/) and China air quality on-line monitoring and analysis platform (https://www.aqistudy.cn/) for providing $PM_{2.5}$ and PM_{10} data, Weather Underground (http://wunderground.com/) for providing meteorological data, and NASA (https://modis-atmos.gsfc.nasa.gov/MOD08_M3/index.html) for providing MODIS data. The authors would like to acknowledge Prof. Dora Pancheva, the Editor-in-Chief of the journal and the two anonymous reviewers for their helpful comments and constructive suggestions towards the improvement of an earlier version of the manuscript.

References

Adesina, A.J., Piketh, S., Kumar, K.R., Venkataraman, S., 2017. Characteristics of columnar aerosol optical and microphysical properties retrieved from the sunphotometer and its impact on radiative forcing over Skukuza (South Africa) during 1999–2010. Environ Sci Pollut Res. 24, 16160-16171

Ångström, A., 1961. Techniques of determining the Turbidity of the Atmosphere. Tellus XIII, 214-223.

Bibi, S., Alam, K., Chishtie, F., Bibi, H., 2017. Characterizing of absorbing aerosol types using ground and satellite-based observations over an urban environment. Atmospheric Environment 150, 126-135.

Boiyo R, Kumar KR, Zhao T. 2018. Spatial variations and trends in AOD climatology over East Africa during 2001–2015: A comparative study using three satellite datasets. International Journal of Climatology. https://doi.org/10.1002/joc.5446.

Boiyo, R., Kumar, K.R., Zhao, T., Guo, J., 2019. A 10-year record of aerosol optical properties and radiative forcing over three environmentally distinct AERONET sites in Kenya, East Africa. Journal of Geophysical Research-Atmospheres 124, 1596-1617.

Carabali, G., Estevez, H.R., Valdes-Barron, M., et al., 2017. Aerosol climatology over the Mexico City basin: Characterization of optical properties. Atmospheric Research 194, 190-201.

Charlson RJ, Schwartz SE, Hales JM, Cess RD, Coakley JA, Hansen JE, Hofmann DJ. 1992. Climate Forcing by Anthropogenic Aerosols. Science. 255: 423–430. https://doi.org/10.1126/science.255.5043.423.

Che, H., Xia, X., Zhu, J., Li, Z., Dubovik, O., Holben, B.N., et al., 2013. Column aerosol optical properties and aerosol radiative forcing during a serious haze-fog month over the North China Plain in 2013 based on ground-based Sunphotometer measurements. Atmos. Chem. Phys. 14, 2125–2138.

Che, H., Zhang, X. Y., Xia, X., Goloub, P., Holben, B., Zhao, H., Wang, Y., et al., 2015. Ground-based aerosol climatology of China: aerosol optical depths from the China Aerosol Remote Sensing Network (CARSNET) 2002-2013. Atmospheric Chemistry and Physics 15, 7619-7652.

Chen, G., Morawska, L., Zhang, W., Li, S., Cao, W., Ren, H., Wang, B., Wang, H., Knibbs, L.D., Williams, G., Guo, J., Guo, Y., 2018. Spatiotemporal variation of PM_1 pollution in China. Atmospheric Environment 178, 198-205.

Chen, P., Kang, S., Yang, J., Pu, T., Li, C., Guo, J., Tripathi, L., 2019. Spatial and temporal variations of gaseous and particulate pollutants in six sites in Tibet, China during 2016-2017. Aerosol and Air Quality Research 19, 516-527.

Eck, T.F., Holben, B.N., Reid, J.S., Dubovik, O., Smirnov, A., O'Neill, N. T., et al., 1999. Wavelength dependence of the optical depth of biomass burning, urban, and desert dust aerosols. Journal of Geophysical Research. https://doi.org/10.1029/1999JD900923.

Gobbi, G.P., Kaufman, Y.J., Koren, I., Eck, T.F., 2007. Classification of aerosol properties derived from AERONET direct sun data. Atmospheric Chemistry and Physics Discussions, 6, 8713–8726. https://doi.org/10.5194/acpd-6-8713-2006.

Han, L. J., W. Q. Zhou, W. F. Li, L. Li, 2014. Impact of urbanization level on urban air quality: A case of fine particles ($PM_{2.5}$) in Chinese cities. Environ.Pollut., 194, 163-170.

Hou, X., Zhu, B., Kumar, K.R., Lu, W., 2019. Inter-annual variability in fine particulate matter pollution over China during 2013-2018: Role of meteorology. Atmospheric Environment 214, 116842.

IPCC, 2013: Climate Change. 2013: The Physical Science Basis. Contribution of Working Group I to the Fifth 4 Assessment Report of the Intergovernmental Panel on Climate Change [Stocker, T. F., D. Qin, G.-K.5 Plattner, M. Tignor, S. K. Allen, J. Boschung, A. Nauels,Y. Xia, V. Bex and P. M. Midgley (Eds.)].6 Cambridge University Press, Cambridge, United Kingdom And New York, NY, USA, 1535. https://doi.org/ 7 10.1017/CBO9781107415324.

Kalluri, R.O.K., Gugamsetty, B., Kotalo, R.G., Nagireddy, S.K.R., et al., 2016. Direct radiative forcing properties of atmospheric aerosols over semi-arid region, Anantapur in India. Science of the Total Environment 566-567, 1002-1013.

Kang, N., Kumar, K.R., Hu, K., Yu, X., and Yin, Y., 2016a. Long-term (2002–2014) evolution and trend in Collection 5.1 Level-2 aerosol products derived from the MODIS and MISR sensors over the Chinese Yangtze River Delta. Atmospheric Research. 181, 29–43.

Kang, N., Kumar, K.R., Yu, X., Yin, Y., 2016b. Column-integrated aerosol optical properties and direct radiative forcing over the urban-industrial megacity Nanjing in the Yangtze River Delta, China. Environmental Science and Pollution Research 23, 17532-17552.

Kaskaoutis, D.G., Badarinath, K.V.S., Kharol, S.K., Sharma, A.R., Kambezidis, H.D., 2009. Variations in the aerosol optical properties and types over the tropical urban site of Hyderabad, India. Journal of Geophysical Research-Atmospheres, 114(22), 1–20.

Kaskaoutis, D.G., Kambezidis, H.D., Hatzianastassiou, N., Kosmopoulos, P.G., Badarinath, K. V. S., 2007. Aerosol climatology: dependence of the Angstrom exponent on wavelength over four AERONET sites. Atmos. Chem. Phys. Discuss. 7, 7347–7397. https://doi.org/10.5194/acpd-7-7347-2007.

Kaskaoutis, D.G., Kharol, S.K., Sinha, P.R., Singh, R.P., Kambezidis, H.D., Rani Sharma, A., Badarinath, K.V.S., 2011. Extremely large anthropogenic-aerosol contribution to total aerosol load over the Bay of Bengal during winter season. Atmospheric Chemistry and Physics.11, 7097–7117. https://doi.org/10.5194/acp-11-7097-2011.

Kumar KR, Kang N, Yin Y. 2018. Classification of key aerosol types and their frequency distributions based on satellite remote sensing data at an industrially polluted city in the Yangtze River Delta, China. International Journal of Climatology. 38(1): 320-336. https:// doi.org/ 10.1002/joc.5178.

Kumar, K.R., Kang, N., Sivakumar, V., Griffith D., 2017. Temporal characterisitics of columnar aerosol optical properties and radiative forcing (2011-2015) measured at AERONET's Pretoria_CSIR_DPSS site in South Africa. Atmospheric Environment. 165, 274-289.

Kumar, K.R., Sivakumar, V., Reddy, R.R., Gopal, K.R., Adesina, A.J., 2013. Inferring wavelength dependence of AOD and Ångström exponent over a sub-tropical station in South Africa using AERONET data: Influence of meteorology, long-range transport and curvature effect. Science of the Total Environment. 461–462, 397–408.

Kumar, K.R., Sivakumar, V., Yin, Y., Reddy, R.R., Kang, N., Diao, Y., Adesina, A.J., Yu, X., 2014. Long-term (2003-2013) climatological trends and variations in aerosol optical parameters retrieved from MODIS over three stations in South Africa. Atmos. Environ. 95, 400–408.

Kumar, K.R., Yin, Y., Sivakumar, V. N., Yu., X., Diao Y., Adesina A. J., Reddy, R.R., 2015. Aerosol climatology and discrimination of aerosol types retrieved from MODIS, MISR and OMI over Durban (29.88°S, 31.02°E), South Africa. Atmospheric Environment. 117, 9–18.

Pace, G., Sarra, A., Meloni, D., Piacentino, S., Chamard, P., 2006. Aerosol Optical Properties at Lampedusa (Central Mediterranean). Influence of Transport and Identification of Different Aerosol Types. Atmospheric Chemistry and Physics Discussions. 5: 4929–4969. https:// doi.org/10.5194/acpd-5-4929-2005.

Patel, P.N., Dumka, U.C., Kaskaoutis, D.G., Babu, K.N., Mathur, A.K., 2017. Optical and radiative properties of aerosols over Desalpar, a remote site in western India: Source identification, modification processes and aerosol type discrimination. Science of the Total Environment, 575, 612–627.

Ramanathan V, Crutzen PJ, Kiehl JT, Rosenfeld D. 2001. Aerosols, Climate, and the Hydrological Cycle. Science (New York, N.Y.). 294: 2119–2124. https:// doi.org/10.1126/science.1064034.

Rosenfeld D. 2000. Suppression of Rain and Snow by Urban and Industrial Air Pollution. Science 287: 1793–1796. https:// doi.org/10.1126/science.287.5459.1793.

Schuster GL, Dubovik O, Holben BN, 2006. Angstrom exponent and bimodal aerosol size distributions. J Geophys Res Atmos 111(D7), doi:10.1029/2005JD006328.

Sinha, P.R., Kaskaoutis, D.G., Manchanda, R.K., and Sreenivas, S. (2012). Characteristics of aerosols over Hyderabad in southern Peninsular India: synergy in the classification techniques. Anna. Geophys. 30: 1393–1410.

Srivastava, A.K., Yadav, V.,Pathak, V., Singh, S., Tiwari, S., Bisht, D., Goloub, T., 2014. Variability in radiative properties of major aerosol types: A year long study over Delhi-An urban station in Indo-Gangetic Basin. Science of Total Environment 473-474, 659-666.

Sumesh, R.K., Rajeevan, K., Resmi, E.A., Unnikrishnan, C. K., 2017. Particulate matter concentrations in the southern tip of India: Temporal variations, meteorological influences, and source identification. Earth System Environment 13, 1-18.

Tao, J., Gao, J., Zhang, L., Zhang, R., Che, H., Zhang, Z., Lin, Z., Jing, J., Cao, J., Hsu, S.C., 2014. PM2.5 pollution in a megacity of southwest China: Source apportionment and implication. Atmospheric Chemistry and Physics 14, 8679-8699.

Tiwari, S., Hopke, P.K., Pipal, A.S., Srivastava, A.K., Bisht, D.S., Tiwari, S., Singh, A.K., Soni, V.K., Attri, S.D., 2015. Intra-urban variability of particulate matter ($PM_{2.5}$ and PM_{10}) and its relationship with optical properties of aerosols over Delhi, India. Atmospheric Resarch 166, 223-232.

Wang, Y.G., Ying, Q., Hu, J.L., Zhang, H.L., 2014. Spatial and temporal variations of six criteria air pollutants in 31 provincial capital cities in China during 2013-2014. Environment International 73, 413-422.

Wang, Y.Q., Zhang, X.Y., Draxler, R.R., 2009. TrajStat: GIS-based software that uses various trajectory statistical analysis methods to identify potential sources from long-term air pollution measurement data. Environmental Modeling Software 24, 938-939.

Yu, X., Kumar, K.R., Lü, R., Ma, J., 2016a., Changes in column aerosol optical properties during extreme haze-fog episodes in January 2013 over urban Beijing. Environmental Pollution, 210, 217–226. https://doi.org/10.1016/j.envpol.2015.12.021.

Yu, X., Lu, R., Kumar, K.R., Ma, J., Zhang, Q., Jiang, Y., Kang, N., Yang, S.,Wang, J., Li, M., 2016b. Dust aerosol properties and radiative forcing observed in spring during 2001–2014 over urban Beijing, China. Environ. Sci. Pollut. Res. 23, 15432-15442.

Zhang J, Reid JS. 2010. A decadal regional and global trend analysis of the aerosol optical depth using a data-assimilation grade over-water MODIS and Level 2 MISR aerosol products. Atmospheric Chemistry and Physics. 10, 10949–10963.

Zhang, Y. L., F. Cao, 2015. Fine particulate matter ($PM_{2.5}$) in China at a city level. Sci. Rep., 5, 14884.

Table 1. Inter-annual variations of PM concentrations and aerosol optical properties observed at Nanjing during autumn and winter seasons of 2014-2017.

Year	$PM_{2.5}$		PM_{10}		$PM_{10-2.5}$		$PM_{2.5}/PM_{10}$		AOD_{440}		$AE_{440-870}$	
	Aut	Win	Aut	Win	Aut	Win	Aut	Win	Aut	Win	Aut	Win
2014	58.9±27.5	78.6±41.6	111.5±47.6	135.6±57.1	48.1±19.2	58.1±27.7	0.59±0.10	0.57±0.14	0.94±0.44	0.72±0.30	1.05±0.20	1.02±0.21
2015	47.9±28.2	81.2±41.5	87.2±43.2	128.0±52.2	39.4±20.0	46.8±20.9	0.54±0.12	0.62±0.13	0.97±0.31	0.86±0.45	1.14±0.23	0.96±0.29
2016	33.7±19.1	61.7±30.9	65.8±34.5	101.5±46.5	32.1±17.4	39.8±19.3	0.51±0.10	0.60±0.10	-	0.67±0.31	-	1.30±0.22
2017	35.2±21.9	75.7±50.4	69.6±38.9	118.3±64.1	34.3±20.2	42.6±24.4	0.50±0.12	0.63±0.15	0.60±0.32	0.62±0.34	1.25±0.19	1.29±0.19
Mean	45.8±29.3	74.1±42.4	83.5±45.0.	120.9±56.6	37.7±19.8	46.8±24.2	0.53±0.12	0.60±0.13	0.84±0.26	0.72±0.22	1.15±0.14	1.14±0.20

Table 2. Statistics obtained from the linear regression fitting between $PM_{2.5}$ and meteorological parameters during the study period. The symbols m, c, r, RMSE, n, and p represents slope, intercept, Pearson's coefficient, root mean square error, total data points, and probability value to test significance of data, respectively. The respective p-values <0.05 and >0.05 indicates significance of data at 95% confidence level and least significant.

Parameters	$PM_{2.5}$ vs Temp	$PM_{2.5}$ vs RH	$PM_{2.5}$ vs WS	$PM_{2.5}$ vs RF	$PM_{2.5}$ vs Vis
m	-0.056	-0.032	-0.011	-0.045	-0.048
c	14.791	76.603	2.985	8.119	8.681
r	-0.28	-0.09	-0.37	-0.22	-0.58
RMSE	7.598	13.251	0.986	7.866	2.704
n	725	725	725	211	725
p	<0.05	<0.05	<0.05	>0.05	<0.05

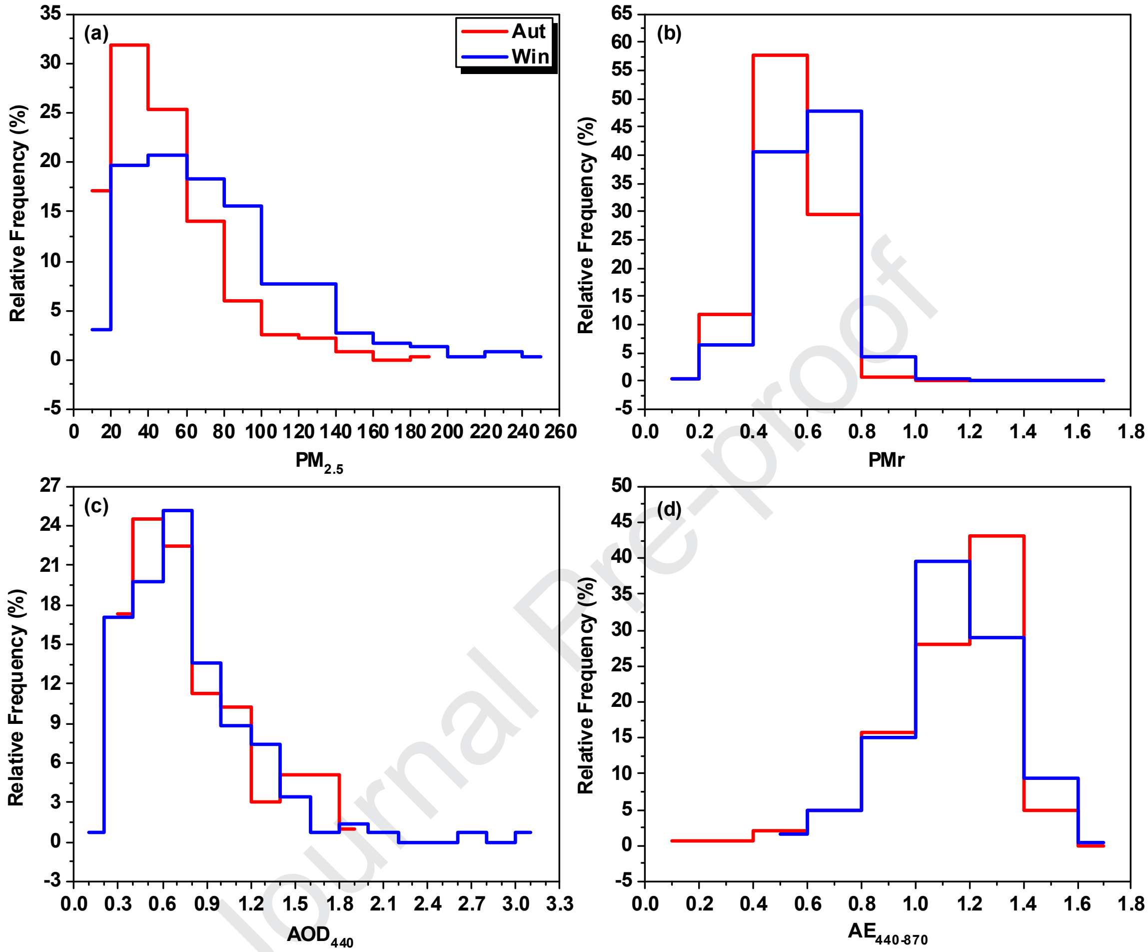

Fig. 1. Relative frequency distributions in measured (a, b) surface and (c, d) column aerosol properties at Nanjing during autumn and winter seasons.

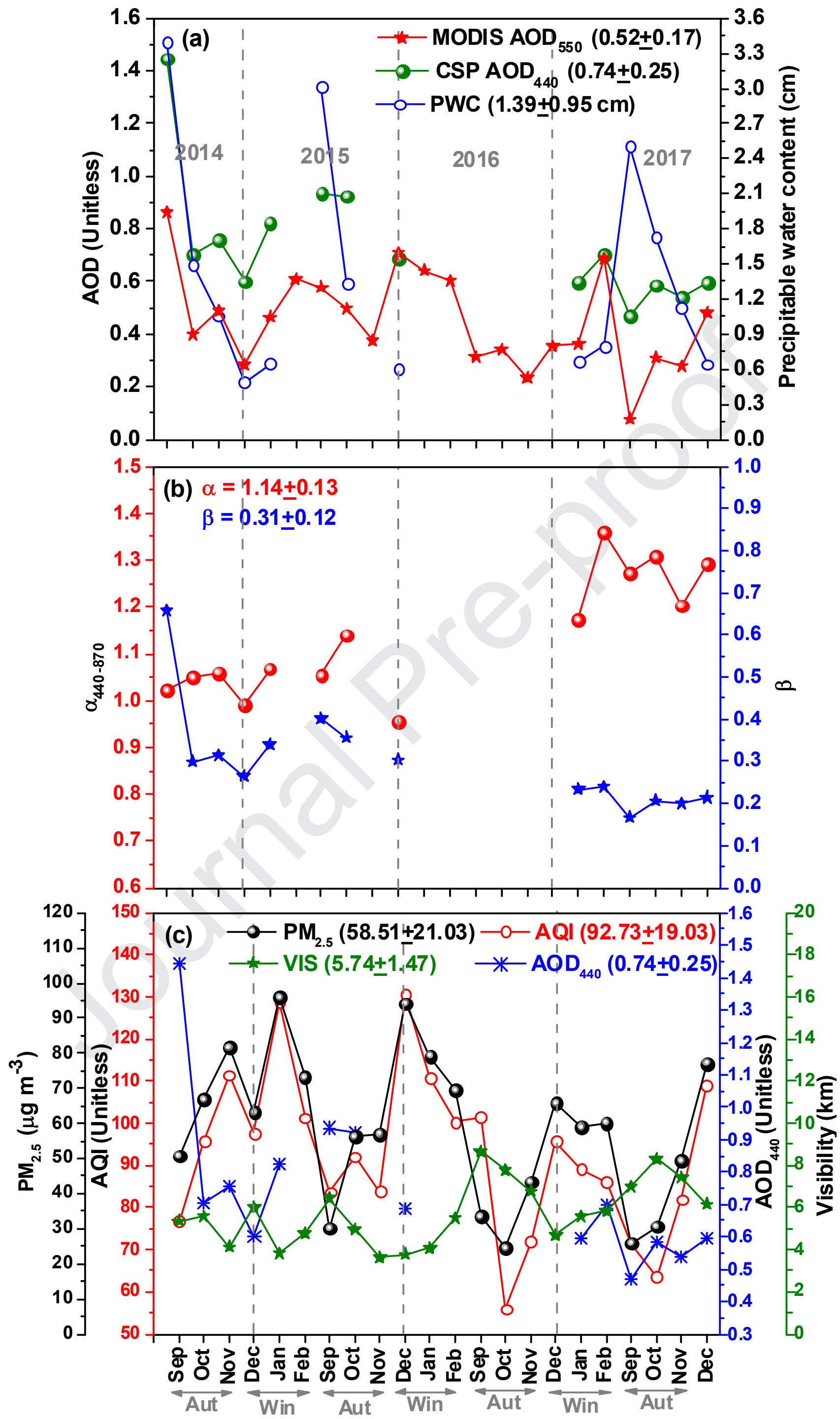

Fig. 2. Temporal variability in (a, b) aerosol optical properties measured from the Sun photometer and surface measured $PM_{2.5}$ concentration at Nanjing during the study period. AQI and visibility are also presented in panel (c) to show their relationship with $PM_{2.5}$ and AOD_{440}.

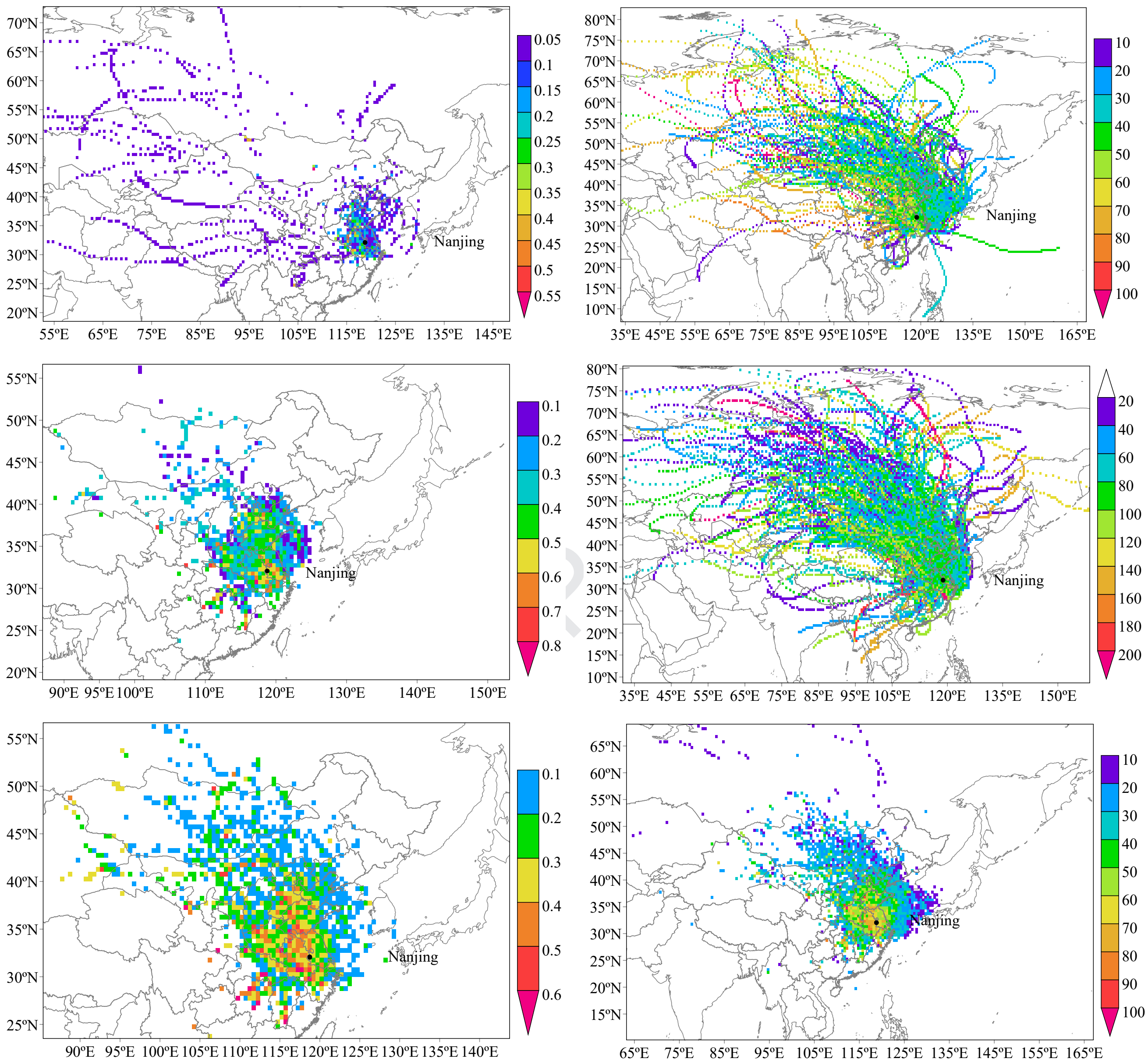

Fig. 3. WPSCF (left) and WCWT (right) maps to identify the sources of $PM_{2.5}$ derived from the PSCF and CWT models arriving Nanjing at a height of 500 m above ground level. The maps are shown for (top) autumn, (middle) winter, and (bottom) all seasons during 2014-2017. The color corresponds to the $PM_{2.5}$ pollutant concentration.

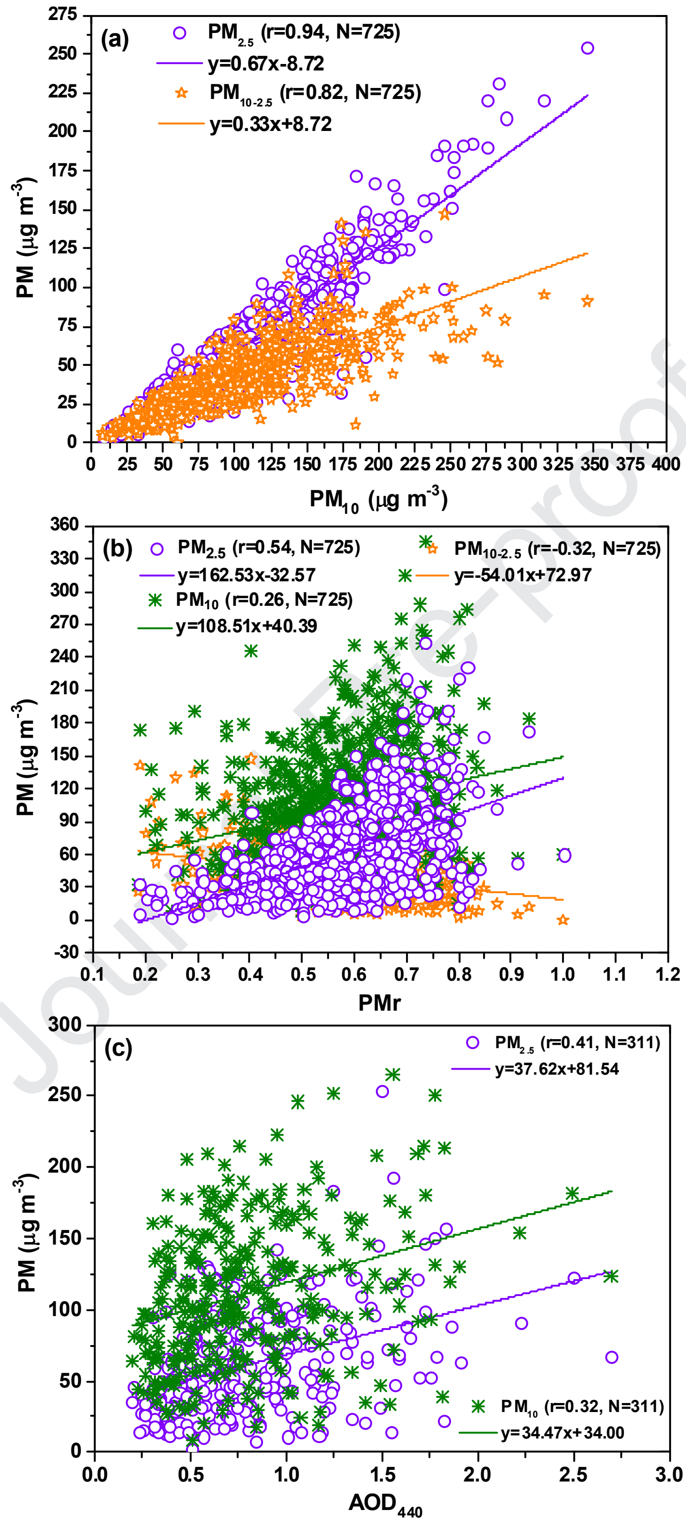

Fig. 4. (a, b) Scatter plots shown for different PM pollutant concentrations and its ratio. (c) Relationship between surface and column aerosol properties observed at Nanjing for the entire study period. The solid lines correspond to the straight lines obtained from the regression fitting. Also, the regression equation, Pearson's correlation coefficient (r) and number of paired data points (N) are given in the panels.

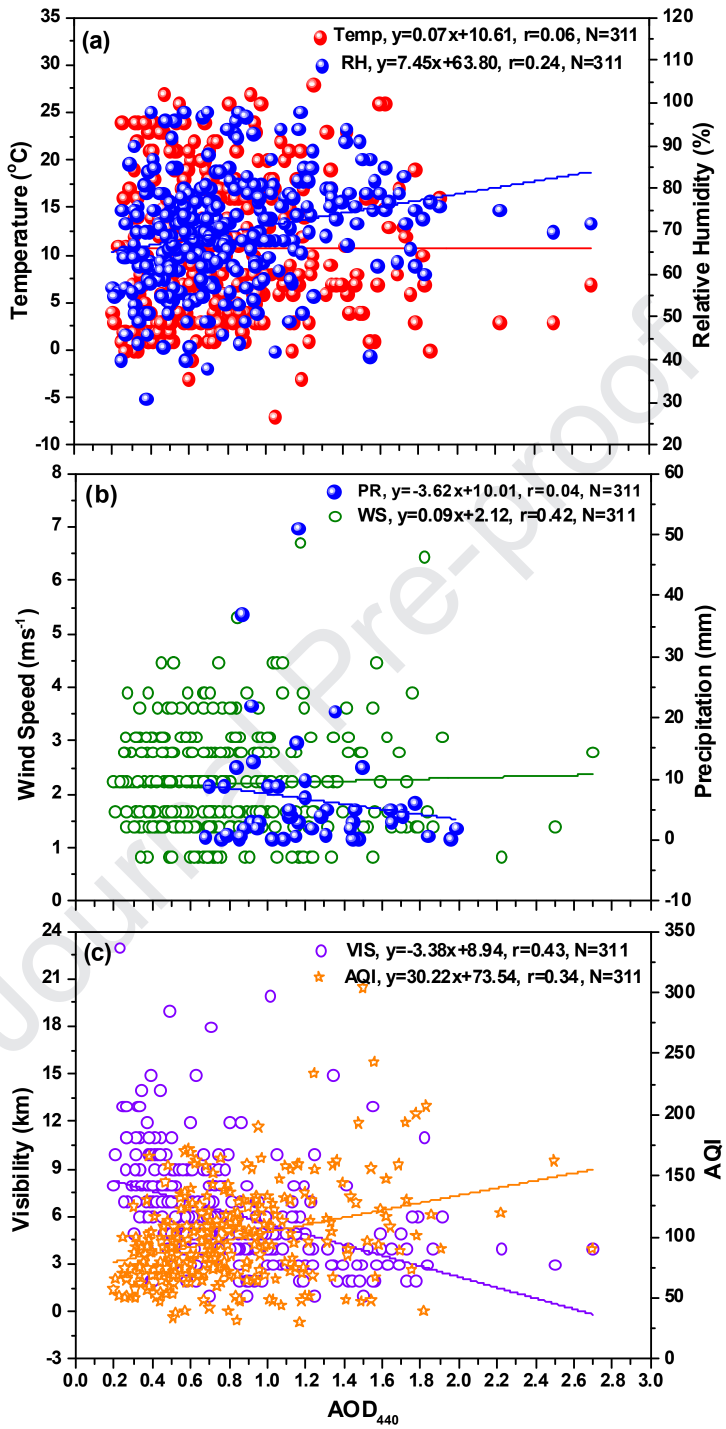

Fig. 5. Association of AOD_{440} with the ground-based measured major meteorological parameters at Nanjing. The regression analysis and its statistics are also presented.

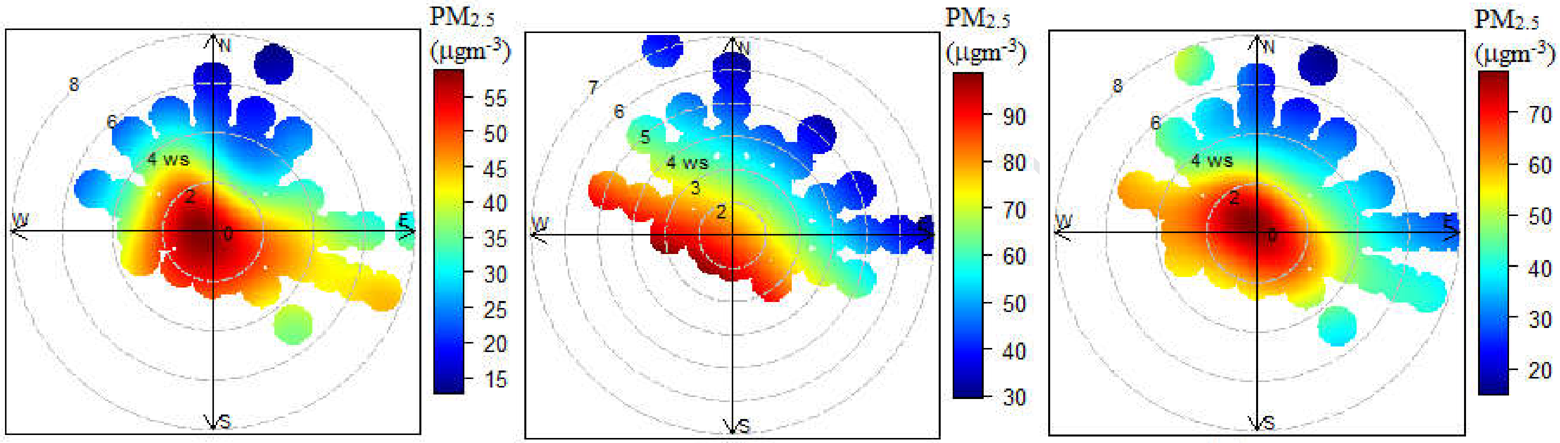

Fig. 6. Concentration bivariate probability function (CBPF) plots of $PM_{2.5}$ concentration during (left) autumn, (middle) winter, and (right) all seasons of 2014-2017. The contour represents the concentration of $PM_{2.5}$ corresponding to the wind speed and direction.

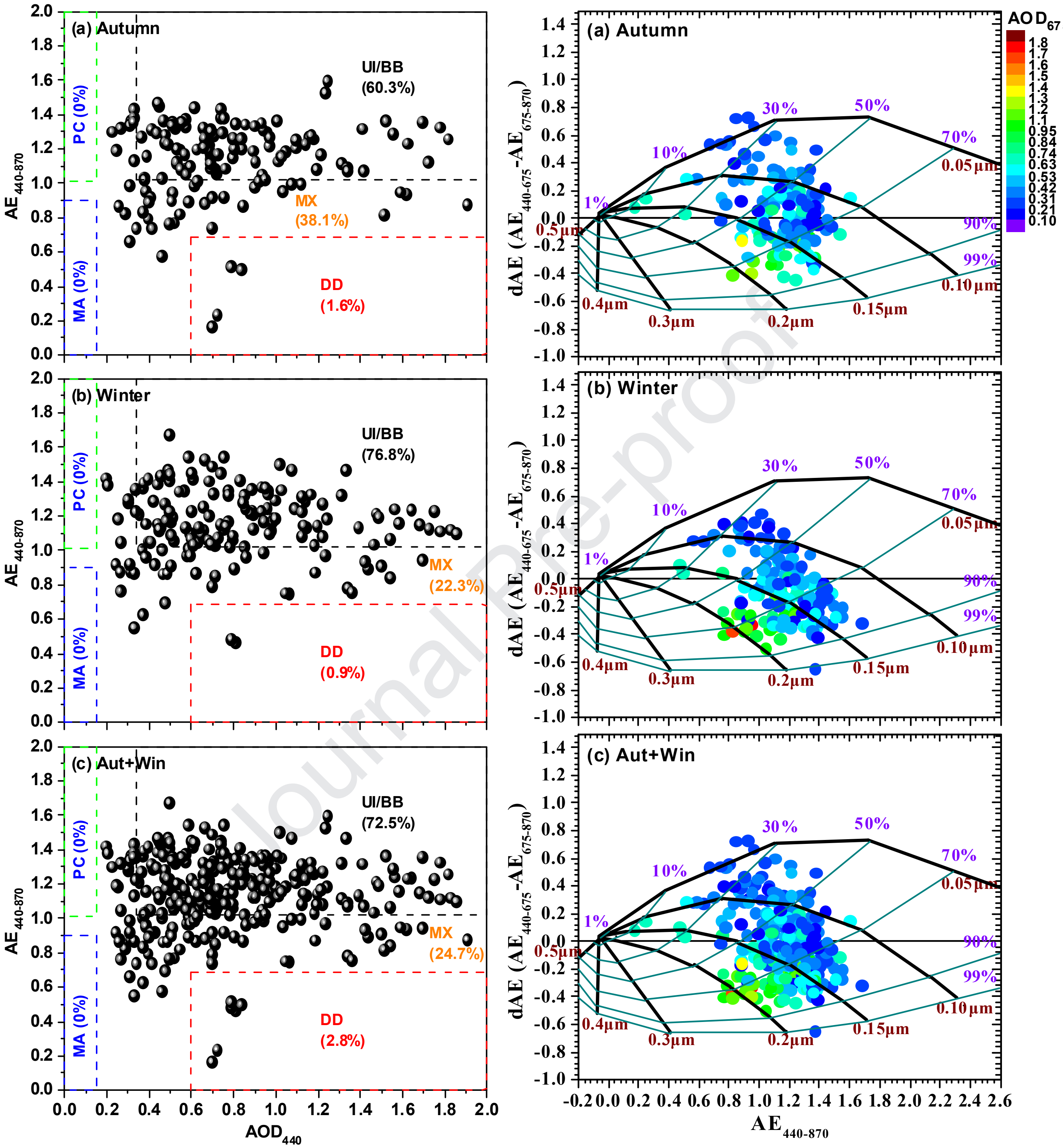

Fig. 7. Aerosol type discrimination (left) and its modification process (right) techniques observed at Nanjing from Sun photometer data during 2014-2017. The major aerosol types are identified and their percentage contributions are also presented.

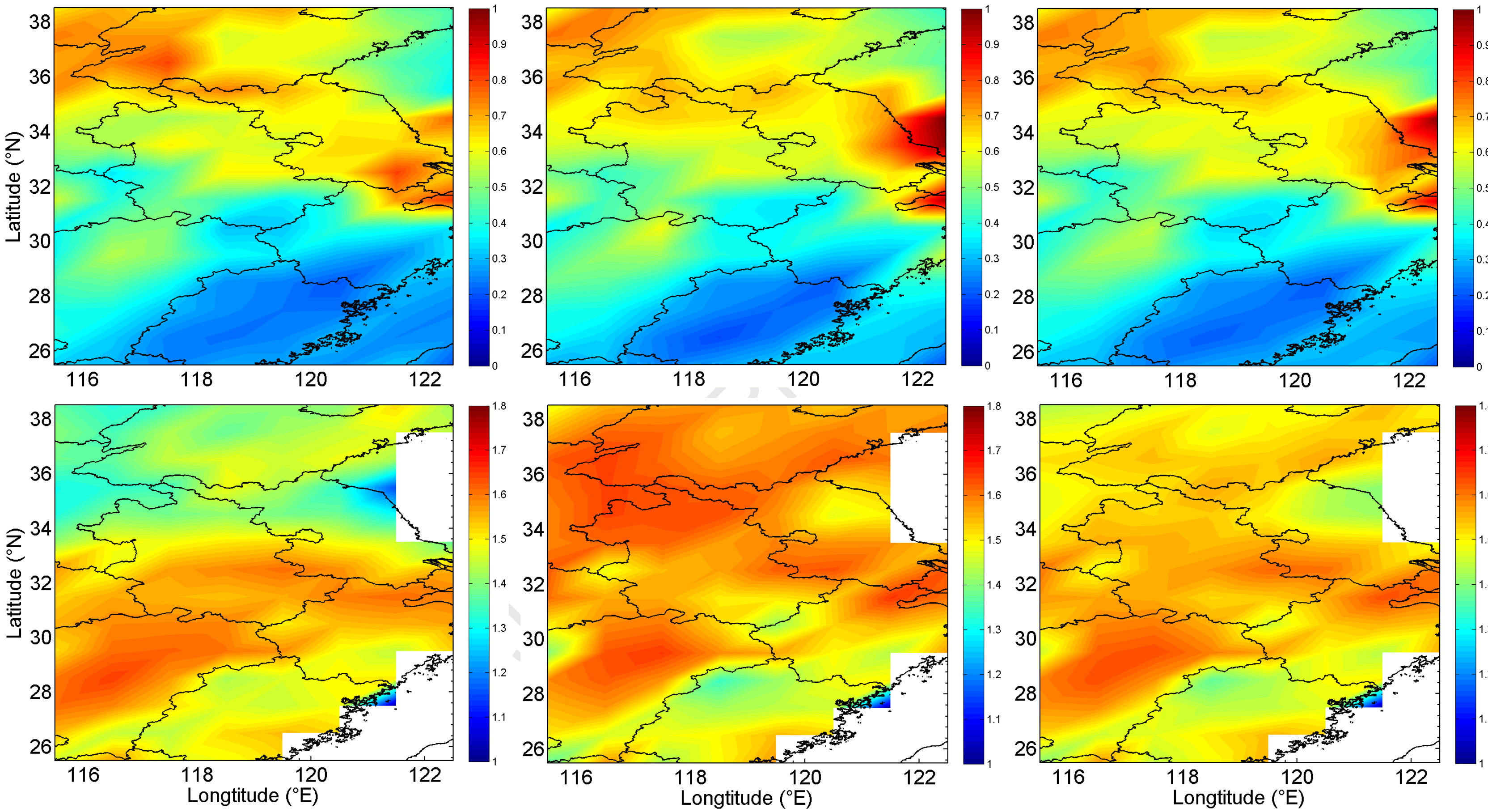

Fig. 8. Spatial distributions of MODIS Aqua satellite-derived AOD_{550} (top panels) and $AE_{440\text{-}660}$ (bottom panels) during 2014-2017. The first, middle, and last panels in two rows corresponds to the autumn, winter and autumn+winter, respectively observed over East China. There are no units for AOD and AE.

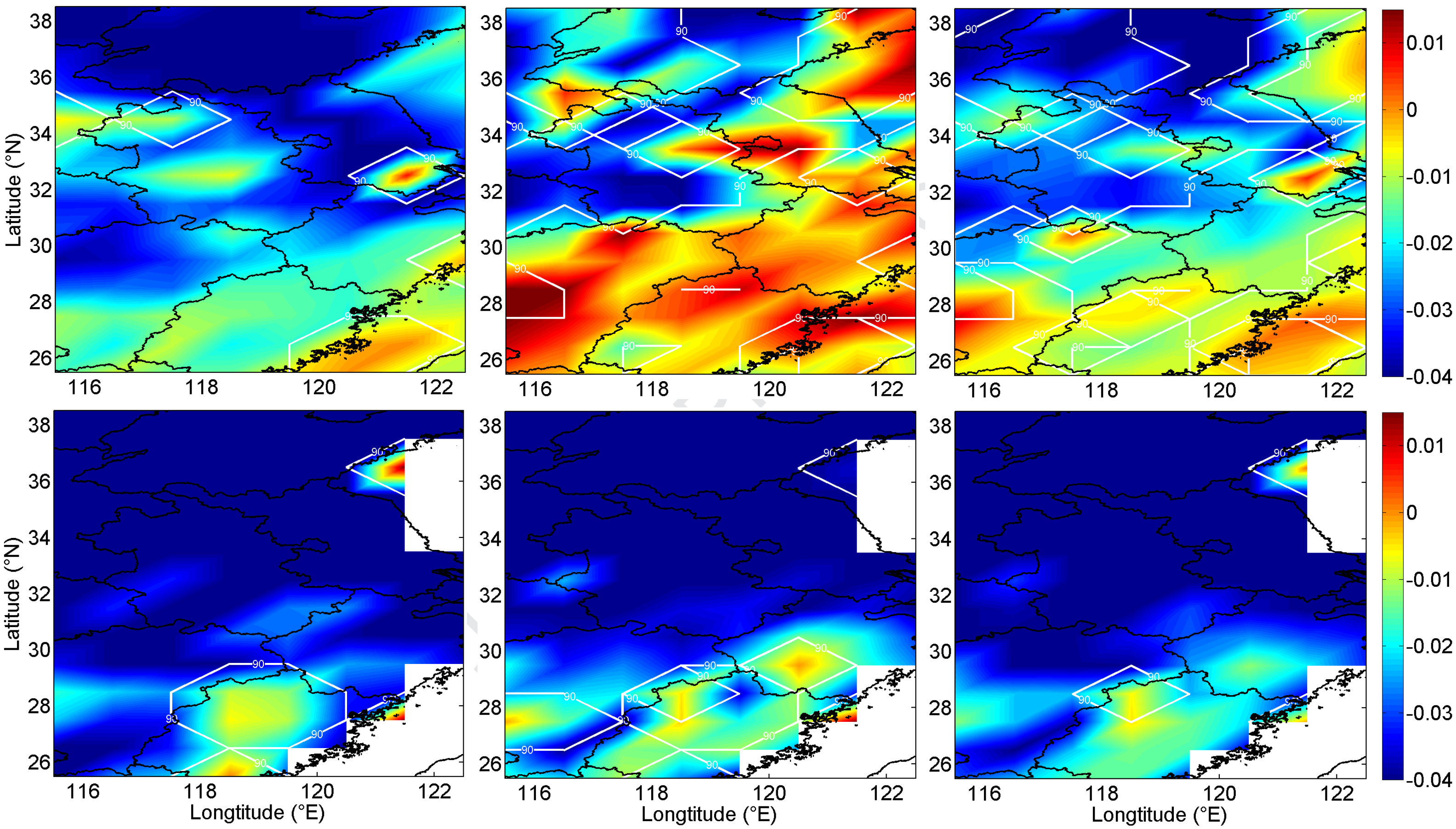

Fig. 9. Spatial distributions of trends observed in AOD_{550} (top panels) and $AE_{440-660}$ (bottom panels) derived from the MODIS Aqua satellite during 2014-2017. The first, middle, and last panels in two rows corresponds to the autumn, winter and autumn+winter, respectively observed over East China. There are no units for the observed trends in AOD and AE. The white lines in all panels represent trends significant at 90% confidence levels and rest is least significant. The positive and negative values in color scale correspond to the respective trends.

RESEARCH HIGHLIGHTS

1. Quantification of PM concentrations and air quality during autumn and winter seasons.
2. The concentrations of $PM_{2.5}$ found maximum in winter relative during autumn.
3. AOD showed high in autumn clearly demonstrates negative correlation with PM.
4. The CWT analysis revealed a significant contribution to PM during winter.
5. The meteorological variables showed negative relationship with PM in all seasons.